GRANULAR MATTER 2(3) 2000, in press.

Macroscopic material properties from quasi-static, microscopic simulations of a two-dimensional shear-cell

Marc Lätzel, Stefan Luding, and Hans J. Herrmann

Abstract One of the essential questions in the area of granular matter is, how to obtain macroscopic tensorial quantities like stress and strain from "microscopic" quantities like the contact forces in a granular assembly. Different averaging strategies are introduced, tested, and used to obtain volume fractions, coordination numbers, and fabric properties. We derive anew the non-trivial relation for the stress tensor that allows a straightforward calculation of the mean stress from discrete element simulations and comment on the applicability. Furthermore, we derive the "elastic" (reversible) mean displacement gradient, based on a best-fit hypothesis. Finally, different combinations of the tensorial quantities are used to compute some material properties.

The bulk modulus, i.e. the stiffness of the granulate, is a linear function of the trace of the fabric tensor which itself is proportional to the density and the coordination number. The fabric, the stress and the strain tensors are *not* co-linear so that a more refined analysis than a classical elasticity theory is required.

1 Introduction

Macroscopic continuum equations for the description of the behavior of granular media rely on constitutive equations for stress, strain, and other physical quantities describing the state of the system. One possible way of obtaining an observable like the stress is to perform discrete particle simulations [1, 2] and to average over the "microscopic" quantities in the simulation, in order to obtain an averaged macroscopic quantity. In the literature, slightly different definitions for stress and strain averaging procedures can be found [3–12].

Received: 23 July 1999

Marc Lätzel, Stefan Luding, and Hans J. Herrmann

Institute for Computer Applications 1,
Pfaffenwaldring 27,
70569 Stuttgart, GERMANY
Correspondence to: m.laetzel@ica1.uni-stuttgart.de

We thank S. Diebels, W. Ehlers, D. Schaeffer, J. Socolar, O. Tsoungui and W. Volk for helpful and inspiring discussions. Also we appreciate the cooperation with B. Behringer and D. Howell and acknowledge the support of the the German National Science Foundation DFG through the research group 'Modellierung kohäsiver Reibungsmaterialien'.

The outline of this study is as follows. In section 2 the discrete element simulation method is discussed and, in section 3 some averaging methods are introduced and applied to a scalar quantity, namely the volume fraction. Section 4 contains the definitions and averaging strategies for fabric, stress, and elastic strain and in section 5 some material properties are extracted from the results obtained in section 4.

2 Modelling discrete particles

The elementary units of granular materials are mesoscopic grains. In order to account for the excluded volume, one can assume that the grains are impenetrable but deform under stress. Since the realistic modelling of the deformations of the particles in the framework of a continuum theory [13, 14] would be much too complicated, we relate the interaction force to the overlap δ of two particles. Note that the evaluation of the inter particle forces based on the overlap may not be sufficient to account for the nonlinear stress distribution inside the particles. Consequently, our results presented below are of the same quality as this basic assumption.

The force laws used are material dependent, involving properties such as Young's modulus of elasticity, and have to be validated by comparison with experimental measurements [15–17].

When all forces $\boldsymbol{f}_i$ acting on the particle i, either from other particles, from boundaries or from external forces, are known, the problem is reduced to the integration of Newton's equations of motion for the translational and the rotational degrees of freedom

$$m_i \frac{\mathrm{d}^2}{\mathrm{d}t^2}\boldsymbol{r}_i = \boldsymbol{f}_i \ , \quad \text{and} \quad I_i \frac{\mathrm{d}^2}{\mathrm{d}t^2}\boldsymbol{\Phi}_i = \boldsymbol{M}_i \ . \tag{1}$$

The mass of particle i with diameter d_i is m_i, and its moment of inertia is $I_i = q_i m_i (a_i)^2$, with the radius $a_i = d_i/2$ and the dimensionless shape factor q_i. The vectors $\boldsymbol{r}_i$ and $\boldsymbol{\Phi}_i$ give the position and the orientation angles of particle i, respectively. In our model attractive forces and the presence of other phases are neglected, we focus on "dry granular media". Particle-particle interactions are short range and active on contact only. The total force (torque) due to other particles is thus $\boldsymbol{f}_i = \sum_c \boldsymbol{f}_i^c$ ($\boldsymbol{M}_i = \sum_c \boldsymbol{M}_i^c$), where the sum runs over all contacts of particle i. The torque $\boldsymbol{M}_i^c = \boldsymbol{l}_i^c \times \boldsymbol{f}_i^c$ is related to the force $\boldsymbol{f}_i^c$ via the cross product with the branch vector $\boldsymbol{l}_i^c$ from the particle center to the point of contact c. Eq. (1) consists

of six scalar equations in three dimensions and reduces to three equations in two dimensions (2D), two for the linear and one for the rotational degree of freedom. In the following the force laws for $\boldsymbol{f}_i^c$ accounting for excluded volume, dissipation, and friction are introduced.

2.1 Force laws

The particles i and j interact only when they are in contact so that their overlap $\delta = \frac{1}{2}(d_i + d_j) - (\boldsymbol{r}_i - \boldsymbol{r}_j) \cdot \boldsymbol{n}$ is positive, with the unit vector $\boldsymbol{n} = (\boldsymbol{r}_i - \boldsymbol{r}_j)/|\boldsymbol{r}_i - \boldsymbol{r}_j|$ that points from j to i. The symbol '$\cdot$' denotes the scalar product of vectors or, more generally, the order-reduction by one for each of two tensors.

The first contribution to the force acting on particle i from j is an elastic repulsive force

$$\boldsymbol{f}_{\mathrm{n,el}} = k_n \delta \boldsymbol{n} \ , \tag{2}$$

where k_n is proportional to the material's modulus of elasticity with units $[N/m]$. Since we are interested in disks rather than spheres, we use a linear spring that follows Hooke's law, whereas in the case of elastic spheres, the Hertz contact law would be more appropriate [18,19].

The second contribution, a viscous dissipation, is given by the damping force in the normal direction

$$\boldsymbol{f}_{\mathrm{n,diss}} = \gamma_n \dot{\delta} \boldsymbol{n} \ , \tag{3}$$

where γ_n is a phenomenological normal viscous dissipation coefficient with units $[\mathrm{kg\,s^{-1}}]$ and $\dot{\delta} = -\boldsymbol{v}_{ij} \cdot \boldsymbol{n}$ the relative velocity in the normal direction $\boldsymbol{v}_{ij} = \boldsymbol{v}_i - \boldsymbol{v}_j$.

The third contribution to the contact force – accounting for tangential friction – can be chosen in the simplest case, according to Coulomb, as $\boldsymbol{f}_{\mathrm{t,friction}} \leq -\mu |\boldsymbol{f_n}| \boldsymbol{t}$, where μ is the friction coefficient and $\boldsymbol{t} = \dot{\boldsymbol{\xi}}/|\dot{\boldsymbol{\xi}}|$ is the tangential unit-vector parallel to the tangential component of the relative velocity $\dot{\boldsymbol{\xi}} = \boldsymbol{v}_{ij} - (\boldsymbol{v}_{ij} \cdot \boldsymbol{n})\boldsymbol{n}$. Because this non-smooth ansatz leads to numerical problems for small $\dot{\boldsymbol{\xi}}$ a regularizing viscous force $\boldsymbol{f}_{\mathrm{t,viscous}} = -\gamma_t \dot{\boldsymbol{\xi}}$ is added. The two forces are combined by taking the minimum value

$$\boldsymbol{f}_{\mathrm{t}} = -\min(|\gamma_t \dot{\boldsymbol{\xi}}|, |\mu \boldsymbol{f_n}|) \boldsymbol{t} \ . \tag{4}$$

The effect of a more realistic tangential force law according to Cundall and Strack [20] will be reported elsewhere [21]. Due to the boundary conditions introduced below, it is also necessary to account for the friction with the bottom

$$\boldsymbol{f}_{\mathrm{b}} = -\mu_{\mathrm{b}} m g \hat{\boldsymbol{v}} \ , \tag{5}$$

with the unit vector in the direction of the particles velocity $\hat{\boldsymbol{v}} = \boldsymbol{v}/|\boldsymbol{v}|$. The effect of a bottom friction was discussed also in [22]. In summary, we combine the forces and use

$$\boldsymbol{f}_i = \sum_c (\boldsymbol{f}_{\mathrm{n,el}} + \boldsymbol{f}_{\mathrm{n,diss}} + \boldsymbol{f}_{\mathrm{t}}) + \boldsymbol{f}_{\mathrm{b}} \tag{6}$$

for the forces acting on particle i at its contact c with particle j.

2.2 Model system

In the simulations presented in this study, a two-dimensional Couette shear-cell is used, filled with a bidisperse packing of disks, as sketched in Fig. 1. The system undergoes slow shearing introduced by turning the inner ring. The properties of the particles, used for the force laws of subsection 2.1, are summarized in table 1. The boundary conditions are based on an experimental realization [23–25]. For more details on other simulations, see [22,24].

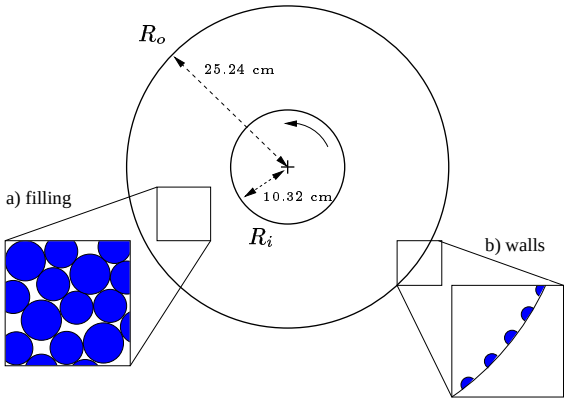

Fig. 1. A schematic plot of the model system

property	values
diameter d_{small}, mass m_{small}	7.42 mm, 0.275 g
diameter d_{large}, mass m_{large}	8.99 mm, 0.490 g
wall-particle diameter d_{wall},	2.50 mm
system/disk-height h	6 mm
normal spring constant k_n	352.1 N/m
normal viscous coefficient γ_n	0.19 kg/s
tangential viscous damping γ_t	0.15 kg/s
Coulomb friction coefficient μ	0.44
bottom friction coefficient μ_b	2×10^{-5}
material density ρ_0	1060 $\mathrm{kg\,m^{-3}}$

Table 1. Microscopic material parameters of the model.

In the simulations different global volume fractions

$$\bar{\nu} = \frac{1}{V_{\mathrm{tot}}} \sum_{p=1}^{N} V^p \tag{7}$$

of the shear-cell are examined. The sum in Eq. (7) runs over all particles p with volume $V^p = \pi h a_p^2$ in the cell with $V_{\mathrm{tot}} = \pi h (R_o^2 - R_i^2)$. In this study $\bar{\nu}$ is varied between 0.8084 and 0.8194, by varying the particle number, see table 2. For the calculation of the global volume fraction, the small particles glued to the wall are counted with half their volume only, and thus contribute with $\bar{\nu}_{\mathrm{wall}} = 0.0047$ to $\bar{\nu}$.

Note that we use the phrases "volume" and "volume fraction" even if, strictly speaking, the unfamiliar terms "disk area" and "area fraction" could be used. The reasons

	global volume fraction $\bar{\nu}$	number of particles small	large	$t_{\max}$ (s)	Δt (s)
A	0.8084	2511	400	335	5
B	0.8103	2520	399	119	1
C	0.8133	2524	404	119	1
D	0.8149	2545	394	119	1
E	0.8180	2538	407	505	5
F	0.8194	2555	399	119	1

Table 2. Details of the simulation runs studied in this paper.

for this choice are: (i) The methods discussed in this study are straightforwardly generalized to three dimensions and (ii) the particles are three dimensional objects with height h anyway, so that the use of the word "volume" is justified.

2.3 Initial conditions and steady state

The simulations are started in a dilute state with an extended outer ring $R_o(t=0) > R_o = 0.2524\,\mathrm{m}$, and the inner ring already rotates counterclockwise with constant angular frequency $\Omega = 2\pi/T_i = 0.1\,\mathrm{s}^{-1}$ and period $T_i = 62.83\,\mathrm{s}$. The extended outer ring is used in order to allow for a random, dilute initial configuration. The desired density is then reached by reducing the volume. The radius of the outer ring is reduced within about two seconds to reach its desired value R_o. Afterwards, the outer ring is kept fixed and the inner ring continues to rotate until at $t = t_{\max}$ the simulation ends. If not explicitly mentioned, averages are performed after about one rotation at $t = 60\,\mathrm{s}$ (to get rid of the arbitrary initial configuration), and during about one rotation, until $t = 119\,\mathrm{s}$.

3 From the micro- to a macro-description

In the previous section, the microscopic point of view was introduced, as used for the discrete element method. Particles are viewed as independent entities which interact when they come in contact. In this framework, the knowledge of the forces at each contact is sufficient to model the dynamics and the statics of the system. Tensorial quantities like the stress or the deformation gradient are not necessary for a discrete modelling. However, subject of current research is to establish a correspondence to continuum theories by computing tensorial quantities like the stress $\boldsymbol{\sigma}$, the strain $\boldsymbol{\varepsilon}$, as well as scalar material properties like, e.g., the bulk and shear moduli [7, 9, 10]. In the course of this process, we first discuss averaging strategies using the material density as an example.

3.1 Averaging strategies

Most of the measurable quantities in granular materials vary strongly on short distances. Thus, computing averages necessitates dealing with or smearing out the fluctuations. In order to suppress the fluctuations, we perform averages in both time and space. This is possible due to the chosen boundary condition. The system can run for long time in a quasi-steady state and, due to the cylindrical symmetry, points at a certain distance R from the origin are equivalent to each other. Therefore, averages are taken over many snapshots in time with time steps Δt and on rings of material at a distance $r = R - R_i$ from the inner ring. The width of the averaging rings is Δr, so that the averaging volume of one ring is $V_r = 2\pi h r \Delta r$. For the sake of simplicity (and since the procedure is not restricted to cylindrical symmetry), the averaging volume is denoted by $V = V_r$ in the following. The rings are numbered from $s = 0$ to $B - 1$, with $B = (R_o - R_i)/\Delta r$, and ring s reaches from $r_s = r - \Delta r/2$ to $r_{s+1} = r + \Delta r/2$. The averaging over many snapshots is somehow equivalent to an ensemble average. However, we remark that different snapshots are not necessarily independent of each other as discussed in subsection 3.4. Also the duration of the simulation maybe not long enough to explore a representative part of the phase space.

The cylindrical symmetry is accounted for by a rotation of all directed quantities like vectors, depending on the cartesian position $\boldsymbol{r}_i = (x_i, y_i)$ of the corresponding particle i. The orientation of particle i is $\phi_i = \arctan(y_i/x_i)$ for $x_i > 0$ and periodically continued for $x_i < 0$ so that ϕ_i can be found in the interval $[-\pi, \pi]$. The vector $\boldsymbol{n}^c$ that corresponds to contact c of particle i is then rotated about the angle $-\phi_i$ from its cartesian orientation before being used for an average. Note that this does *not* correspond to a transformation into orthonormal cylindrical coordinates.

Finally, we should remark that the most drastic assumption used for our averaging procedure is the fact, that all quantities are smeared out over one particle. Since it cannot be the goal to solve for the stress field inside one particle, we assume that a measured quantity is constant inside the particle. This is almost true for the density, but not e.g. for the stress. However, since we average over all positions with similar distance from the origin, i.e. averages are performed over particles with different positions inside a ring, details of the position dependency inside the particles will be smeared out anyway. An alternative approach was recently proposed by I. Goldhirsch [11] who smeared out the averaging quantities along the lines connecting the centers of the particles and weighed the contribution according to the fraction of this line within the averaging volume.

3.2 Volume fractions

The first quantity to measure is the local volume fraction

$$\nu = \nu(r) = \frac{1}{V} \sum_{p \in V} w_V^p V^p \tag{8}$$

with the particle volume V^p. w_V^p is the weight of the particle's contribution to the average.

This formalism can be extended to obtain the mean value of a quantity Q in the following way:

$$Q = \langle Q^p \rangle = \frac{1}{V} \sum_{p \in V} w_V^p V^p Q^p \ , \tag{9}$$

with the pre-averaged particle quantity

$$Q^p = \sum_{c=1}^{\mathcal{C}^p} Q^c \ . \tag{10}$$

with the quantity Q^c attributed to contact c of particle p. In the following the brackets $\langle Q \rangle$ denote the average over a quantity Q of the particles in an averaging volume V.

The simplest choice for w_V^p is to use $w_V^p = 1$, if the center of the particle lies inside the ring, and $w_V^p = 0$ otherwise. This method will be referred to as *particle-center averaging* in the following.

A more complicated way to account for those parts of the particles which lie partially inside a ring is to use only the fraction of the particle volume that is covered by the averaging volume. Since an exact calculation of the area of a disk that lies in an arbitrary ring is rather complicated, we assume that the boundaries of V are locally straight, i.e. we cut the particle in slices, as shown in Fig. 2. This method will be referred to as *slicing* in the following. The error introduced by using straight cuts is well below one per-cent in all situations considered here.

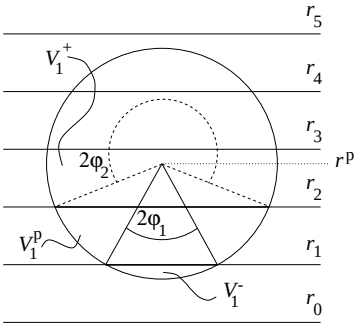

Fig. 2. Schematic plot of a particle p at radial position r^p which is cut into pieces by the boundaries r_s of the averaging volumes. We assume $s = 0, \ldots, m+1$ such that all r_s with $s = 1, \ldots, m$ hit the particle, i.e. $|r^p - r_s| < d/2$.

The volume $V_s^p = w_V^p V^p$ of a particle p which partially lies between r_s and r_{s+1} is calculated by subtracting the external volumes V_s^- and V_s^+ from the particle volume $V^p = \pi h (d/2)^2$ so that

$$\begin{aligned} V_s^p &= V^p - V_s^- - V_s^+ \\ &= h(d/2)^2[\pi - \phi_s + \sin(\phi_s)\cos(\phi_s) \\ &\qquad - \phi_{s+1} + \sin(\phi_{s+1})\cos(\phi_{s+1})] \end{aligned} \tag{11}$$

with $\phi_s = \arccos(2(r^p - r_s)/d)$ and $\phi_{s+1} = \arccos(2(r_{s+1} - r^p)/d)$. The term $(d/2)^2\phi$ is the area of the segment of the circle with angle 2ϕ, and the term $(d/2)^2 \sin(\phi)\cos(\phi)$ is the area of the triangle belonging to the segment. In Fig. 2 the case $s = 1$ is highlighted, and the boundaries between V_s^-, V_s^p, and V_s^+ are indicated as thick solid lines. The two outermost slices $V_0^p = V_1^-$ and $V_s^p = V_{s-1}^+$ have to be calculated separately.

When the two averaging strategies (particle-center and slicing) are compared for different widths Δr of the averaging rings, so that the number of intervals is $B = 20$, 40, or 60. For $\Delta r \approx d_{\mathrm{small}}$ ($B = 20$), the results are almost independent of the averaging procedure. For finer binning $B_s \geq 30$, the slicing procedure converges on a master curve with weak oscillations close to the walls which are due to the wall-induced layering of the particles. The results of the particle-center averaging strongly fluctuate for $B_c \geq 24$. These oscillations come from ordered layers of the particles close to the walls so that the slicing method reflects the real density distribution for fine enough binning. The particle-center method, on the other hand, leads to peaks, where the centers of the particles in a layer are situated and to much smaller densities where few particle centers are found; the particle-center density is obtained rather than the material density.

3.3 Representative elementary volume REV

An important question is, how does the result of an averaging procedure depend on the size of the averaging volume V. We combine time- and space averaging, i.e. we average over many snapshots and over rings of width Δr, so that the remaining "size" of the averaging volume is the width of the rings Δr. In Fig. 3 data for ν at fixed position $R = 0.12$, 0.13, 0.14, and 0.20 m, but obtained with different width Δr, are presented. The positions correspond to $r/d_{\mathrm{small}} \approx 2.2$, 3.6, 4.9, and 13, when made dimensionless with the diameter of the small particles. Both the particle-center method (open symbols) and the slicing method (solid symbols) are almost identical for $\Delta r/d_{\mathrm{small}} \geq 2$, for the larger Δr the averaging volume can partially lie outside of the system. For very small $\Delta r/d_{\mathrm{small}} \leq 0.1$ the different methods lead to strongly differing results, however, the values in the limit $\Delta r \to 0$ are consistent, i.e. independent of Δr besides statistical fluctuations. In the intermediate regime $0.1 < \Delta r/d_{\mathrm{small}} < 2$, the particle-center method strongly varies, while the slicing method shows a comparatively smooth variation.

Interestingly, all methods seem to collapse at $\Delta r_{\mathrm{REV}} \approx d_{\mathrm{small}}$ (and twice this value), nearly to the size of the majority of the particles. For the examined situations, we observe that the particle-center and the slicing method lead to similar results for $0.97 \leq \Delta r_{\mathrm{REV}}/d_{\mathrm{small}} \leq 1.03$. This indicates that the systems (and measurements of system quantities) are sensitive to a typical length scale, which is here somewhat smaller than the mean particle size. When using this special Δr_{REV} value, one has $B = 20$ or $B = 21$ binning intervals. The open question of this being a typical length scale that also occurs in systems with a broader size spectrum, cannot be answered with our setup, due to the given particle-size ratio.

3.4 Time averaging

In order to understand the fluctuations in the system over time, and to test whether subsequent snapshots can be assumed to be independent, the volume fraction ν is displayed for snapshots at different averaging times in Fig. 4.

Changes in density are very weak and mostly occur in the dilated shear zone for small r. From one snapshot to the next, we frequently find, that the configuration in the

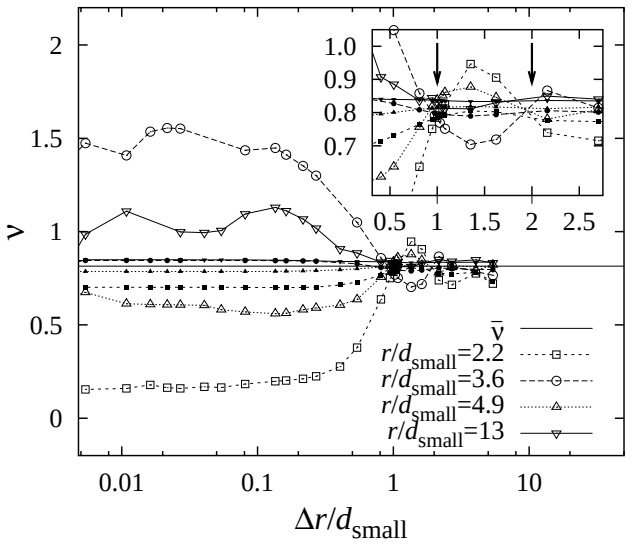

Fig. 3. Volume fraction ν at different distances r from the inner ring, plotted against the width Δr of the averaging ring from simulation D, see table 2. Note that the horizontal axis is logarithmic. The open symbols are results obtained with the particle-center method, the solid symbols are results from the slicing method. The inset is a zoom into the large Δr region, and the arrows indicate the optimal width Δr for the particle-center method for which the results are almost independent of the averaging procedure.

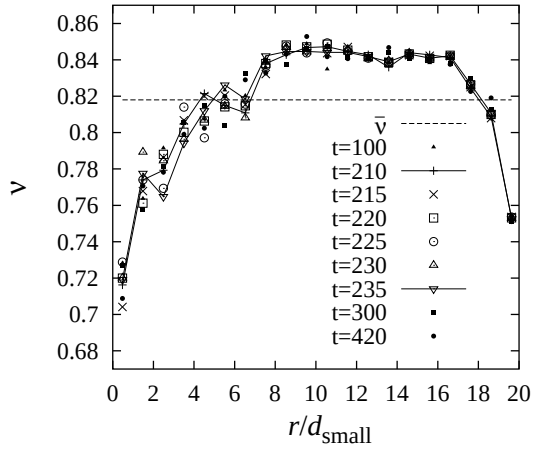

Fig. 4. Volume fraction ν, plotted against the dimensionless distance r/d_{small} from the inner ring, for different times from simulation E. Open symbols belong to six subsequent snapshots with $\Delta t = 5\,\mathrm{s}$, the small, solid symbols are snapshots after longer times.

outer part of the shear cell has not changed, whereas a new configuration is found in the inner part. Only after rather long times does the density change also in the outer part. Thus, simulation results in the outer part are subject to stronger fluctuations because the average is performed over less independent configurations than in the inner part.

4
Macroscopic tensorial quantities

In this section, the averaged, macroscopic tensorial quantities in our model system are presented. The fabric tensor describes the contact network, the stress tensor describes, in this study, the stress due to normal forces, and the deformation gradient is a measure for the corresponding elastic, reversible deformations. A more detailed analysis, where the tangential forces are also taken into account, is in progress [21] and some details in that direction can be found in Refs. [9,10,12]. However, we checked the influence of the tangential forces in our system and found their effect to be always smaller than ten per-cent.

4.1
Micro-mechanical fabric tensor

In assemblies of grains, the forces are transmitted from one particle to the next only at the contacts of the particles. In the general case of non-spherical particles, a packing network is characterized by the vectors connecting the centers of the particles and by the particle-contact vectors. Furthermore, the local geometry of each contact is important [26,27], see Fig. 5. In our case, with spherical particles, the situation is simpler with respect to both the spherical contact geometry and the fabric.

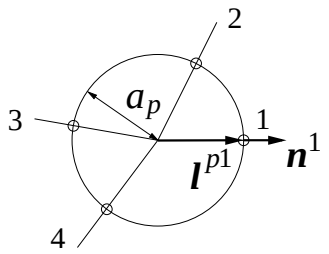

Fig. 5. Schematic plot of a particle with radius a and $\mathcal{C}^p = 4$ contacts as indicated by the small circles. The branch vector $\boldsymbol{l}^{pc}$ and the normal unit vector $\boldsymbol{n}^c$ are displayed at contact $c = 1$.

4.1.1
Fabric tensor for one particle

One quantity that describes the contact configuration of one particle to some extent, is the second order fabric tensor [26,27]

$$\mathbf{F}^p = \sum_{c=1}^{\mathcal{C}^p} \boldsymbol{n}^c \otimes \boldsymbol{n}^c \ , \tag{12}$$

where $\boldsymbol{n}^c$ is the unit normal vector at contact c of particle p with $\mathcal{C}^p$ contacts. The symbol $\otimes$ denotes the dyadic product in this study. Other definitions of the fabric use the so-called branch vector $\boldsymbol{l}^{pc}$ from the center of particle p to its contact c, however, the unit normal and the unit branch vector are related by $a_p \boldsymbol{n} = \boldsymbol{l}^{pc}$ in the case of spheres or disks, so that the definition

$$\mathbf{F}^p = \frac{1}{a_p^2} \sum_{c=1}^{\mathcal{C}^p} \boldsymbol{l}^{pc} \otimes \boldsymbol{l}^{pc} \ . \tag{13}$$

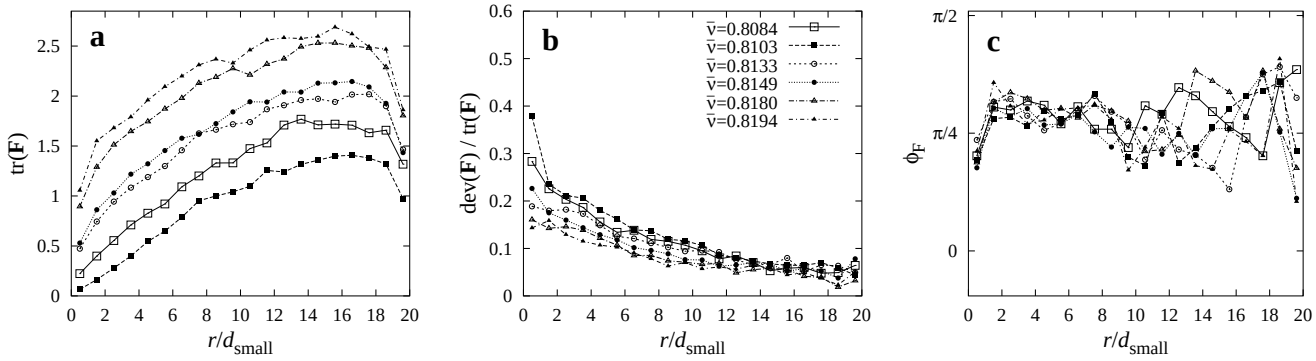

Fig. 6. a-c Plot of (**a**) $F_V = \mathrm{tr}(\mathbf{F})$, (**b**) $F_D/F_V = \mathrm{dev}(\mathbf{F})/\mathrm{tr}(\mathbf{F})$, and (**c**) ϕ_F against the dimensionless distance r/d_{small} from the inner ring. The global volume fraction is given in (**b**) and valid also for (**a**) and (**c**).

is identical to Eq. (12). The fabric tensor in Eq. (12) is symmetric by definition and thus consists of up to three independent scalar quantities in two dimensions. The first of them, the trace (or volumetric part) $F_V = \mathrm{tr}(\mathbf{F}^p) = (F_{\max} + F_{\min})$, is the number of contacts of particle p, with the major and the minor eigenvalues $F_{\max}$ and $F_{\min}$, respectively. One gets from Eqs. (12) or (13) the number of contacts of particle p

$$\mathrm{tr}(\mathbf{F}^p) = \sum_{c=1}^{\mathcal{C}^p} \mathrm{tr}(\boldsymbol{n}^c \otimes \boldsymbol{n}^c) = \mathcal{C}^p \ , \tag{14}$$

since the scalar product of $\boldsymbol{n}^c$ with itself is unity by definition. The second scalar, the deviator $F_D = F_{\max} - F_{\min}$, accounts for the anisotropy of the contact network to first order, and the third, the angle ϕ_F, gives the orientation of the "major eigenvector", i.e. the eigenvector corresponding to $F_{\max}$, with respect to the radial direction. In other words, the contact probability distribution is proportional to the function $[F_V + F_D \cos(2(\phi - \phi_F))]$ [22, 28, 29], when averaged over many particles, an approximation which is not always reasonable [30].

4.1.2 Averaged fabric tensor

Assuming that all particles in V contribute to the fabric with a weight of their volume V^p one has

$$\mathbf{F} = \langle \mathbf{F}^p \rangle = \frac{1}{V} \sum_{p \in V} w_V^p V^p \sum_{c=1}^{\mathcal{C}^p} \boldsymbol{n}^c \otimes \boldsymbol{n}^c \ . \tag{15}$$

The values of F_V, F_D/F_V, and ϕ_F, as obtained from our simulations, are plotted in Figs. 6(a-c). The trace of the fabric tensor and thus the mean number of contacts increases with increasing distance from the inner ring, and is reduced in the vicinity of the walls. With increasing mean density, the trace of $\mathbf{F}$ is systematically increasing, while the deviatoric fraction seems to decrease; this means that a denser system is slightly more isotropic concerning the fabric. The major eigendirection is tilted counterclockwise by somewhat more than $\pi/4$ from the radial outward direction, except for the innermost layer and for the strongly fluctuating outer region.

In analogy to the trace of the fabric for a single particle, the trace of the averaged fabric is

$$\mathrm{tr}(\mathbf{F}) = \frac{1}{V} \sum_{p \in V} w_V^p V^p \mathcal{C}^p = \langle \mathcal{C}^p \rangle \ , \tag{16}$$

which, in the case of a regular, periodic contact network of almost identical particles with $a_p \simeq a$, reduces to the sum over all of particles in V with the prefactor ν defined in Eq. (8). Now, one has a relation between the coordination number, i.e. the mean number of contacts per particle $\mathcal{C} = \mathcal{C}(r) = \langle \mathcal{C}^p \rangle / \nu$, the volume fraction ν, and the averaged fabric $\mathbf{F}$, as a combination of Eqs. (8) and (16):

$$\mathrm{tr}(\mathbf{F}) \simeq \nu \mathcal{C} \ . \tag{17}$$

As a test for the averaging procedure, we plot in Fig. 7 $\mathrm{tr}(\mathbf{F})$ against $\nu\mathcal{C}$ and obtain all data points from all simulations collapsing close to the identity curve. For a theoretical derivation of the small (about 1 per-cent) deviation due to the polydispersity, see Ref. [33].

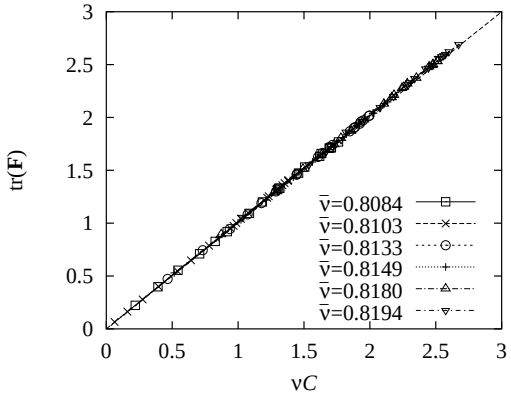

Fig. 7. Trace of the fabric tensor plotted against $\nu\mathcal{C}$ for different packing fractions $\bar{\nu}$. All the points collapse nearby the identity curve (dashed line).

4.2 Micro-mechanical stress tensor

The micro-mechanical stress tensor is derived in a way similar to Ref. [9]. For an arbitrary volume V with surface ∂V, the mean stress is defined as

$$\boldsymbol{\sigma} = \frac{1}{V}\int_V dV'\,\boldsymbol{\sigma}' \;, \tag{18}$$

where $\boldsymbol{\sigma}' = \boldsymbol{\sigma}'(\boldsymbol{x})$ is the position dependent local stress inside V and $\boldsymbol{x}$ is the coordinate integrated over. Note that $\boldsymbol{\sigma}'$ can be a strongly fluctuating function of $\boldsymbol{x}$.

If the stress in the pore-space vanishes, the integral can be split into a sum over the stresses $\boldsymbol{\sigma}^p$, pre-averaged for particles p, with the respective center of mass vectors $\boldsymbol{x}^p$. The mean stress is thus

$$\boldsymbol{\sigma} = \langle\boldsymbol{\sigma}\rangle = \frac{1}{V}\sum_{p\in V} w_V^p V^p \boldsymbol{\sigma}^p = \frac{1}{V}\sum_{p\in V} w_V^p \int_{V^p} dV'\,\boldsymbol{\sigma}' \;, \tag{19}$$

which corresponds to a smearing out of $\boldsymbol{\sigma}'$ over the particles, with $\boldsymbol{\sigma}^p$, the average stress in particle p, to be derived in the following.

One can rewrite the transposed stress tensor so that

$$\boldsymbol{\sigma}^{\mathrm{T}} = \operatorname{grad}\boldsymbol{x}\cdot\boldsymbol{\sigma}^{\mathrm{T}} = \operatorname{div}(\boldsymbol{x}\otimes\boldsymbol{\sigma}) - \boldsymbol{x}\otimes\operatorname{div}\boldsymbol{\sigma} \;, \tag{20}$$

by introducing the unit tensor $\mathbf{I} = \operatorname{grad}\boldsymbol{x}$, and by applying the series rule in the first term on the right hand side. Note that the tensors $\boldsymbol{\sigma}$ on the right hand side are transposed with respect to the left hand side $\boldsymbol{\sigma}^{\mathrm{T}}$. The transposed stress is used for the following operations for the sake of simplicity, however, using the stress directly should lead to the same result. For a more detailed treatment, see Ref. [21]. In static equilibrium and in the absence of body forces, the term $\operatorname{div}\boldsymbol{\sigma}$ on the right hand side vanishes and $\boldsymbol{\sigma}$ is symmetric.

4.2.1 Mean stress for one particle

Using the definition of the transposed stress tensor in Eq. (20) the integral over one particle in Eq. (19) becomes

$$\begin{aligned}(\boldsymbol{\sigma}^p)^{\mathrm{T}} &= \frac{1}{V^p}\int_{V^p} dV'\,\operatorname{div}(\boldsymbol{x}\otimes\boldsymbol{\sigma}') \\ &= \frac{1}{V^p}\int_{\partial V^p} dS\,(\boldsymbol{x}\otimes\boldsymbol{\sigma}')\cdot\boldsymbol{n}\end{aligned} \tag{21}$$

by application of Gauss' theorem. In Eq. (21) dS is the surface element of V^p on ∂V^p and $\boldsymbol{n}$ is the outwards normal unit vector. Using the definition of the stress vector $\boldsymbol{t} = \boldsymbol{\sigma}'\cdot\boldsymbol{n}$ one arrives at

$$(\boldsymbol{\sigma}^p)^{\mathrm{T}} = \frac{1}{V^p}\int_{\partial V^p} dS\;\boldsymbol{x}\otimes\boldsymbol{t} \;. \tag{22}$$

A force $\boldsymbol{f}^c$ acting at a contact c with area δs^c leads to a stress vector $\boldsymbol{t}^c = \boldsymbol{f}^c/\delta s^c$ – even in the limit of small contact area $\delta s^c \ll a_p$. Here, we apply the simplifying assumption that the force $\boldsymbol{f}^c$ is constant on the surface δs^c, i.e. we do not resolve any details at the contact. Explicitly writing the surface element dS as a sum,

$$dS = \sum_{c=1}^{\mathcal{C}^p}\delta(|\boldsymbol{x}-\boldsymbol{x}^c|)\;\delta s^c \;, \tag{23}$$

leads, after integration over the delta functions, to the transposed stress

$$(\boldsymbol{\sigma}^p)^{\mathrm{T}} = \frac{1}{V^p}\sum_{c=1}^{\mathcal{C}^p}\boldsymbol{x}^c\otimes\boldsymbol{f}^c \;. \tag{24}$$

Transposing Eq. (24) leads to an exchange of $\boldsymbol{x}^c$ and $\boldsymbol{f}^c$, and thus to the expression for the mean stress inside particle p:

$$\boldsymbol{\sigma}^p = \frac{1}{V^p}\sum_{c=1}^{\mathcal{C}^p}\boldsymbol{f}^c\otimes\boldsymbol{x}^c \;, \tag{25}$$

which is, at first glance, dependent on the frame of reference associated with the vector $\boldsymbol{x}^c$.

Using vector addition, one has $\boldsymbol{x}^c = \boldsymbol{x}^p + \boldsymbol{l}^{pc}$, with the position vector $\boldsymbol{x}^p$ of particle p and the branch vector $\boldsymbol{l}^{pc}$, pointing from the center of mass of particle p to contact c. Inserting this relation in Eq. (25) leads to

$$\begin{aligned}\boldsymbol{\sigma}^p &= \frac{1}{V^p}\left(\sum_{c=1}^{\mathcal{C}^p}\boldsymbol{f}^c\right)\otimes\boldsymbol{x}^p + \frac{1}{V^p}\sum_{c=1}^{\mathcal{C}^p}\boldsymbol{f}^c\otimes\boldsymbol{l}^{pc} \\ &= \frac{1}{V^p}\sum_{c=1}^{\mathcal{C}^p}\boldsymbol{f}^c\otimes\boldsymbol{l}^{pc} \;,\end{aligned} \tag{26}$$

since the first sum vanishes in static equilibrium, where

$$\sum_{c=1}^{\mathcal{C}^p}\boldsymbol{f}^c = \mathbf{0} \;. \tag{27}$$

4.2.2 Averaged stress tensor

Inserting Eq. (26) in Eq. (19) gives a double sum over all particles with center inside the averaging volume V and all their contacts

$$\boldsymbol{\sigma} = \langle\boldsymbol{\sigma}^p\rangle = \frac{1}{V}\sum_{p\in V} w_V^p \sum_{c=1}^{\mathcal{C}^p}\boldsymbol{f}^c\otimes\boldsymbol{l}^{pc} \;. \tag{28}$$

In other words, stress is pre-averaged over all particles and then averaged over V.

Inserting Eq. (25) in Eq. (19) leads to the mathematically identical sum

$$\boldsymbol{\sigma} = \frac{1}{V}\sum_{p\in V} w_V^p \sum_{c=1}^{\mathcal{C}^p}\boldsymbol{f}^c\otimes\boldsymbol{x}^c \;. \tag{29}$$

This expression can be transformed into a sum over all contacts $c(p,q)\in V$, where at least one of the participating particles p and q lies inside the volume V. The force $\boldsymbol{f}^c = \boldsymbol{f}^{pq} = -\boldsymbol{f}^{qp}$, acting at contact c, from particle q on p is equal, but opposite in direction to the force acting at the same contact from particle p on q, so that

$$\begin{aligned}\boldsymbol{\sigma} &= \frac{1}{V}\sum_{c\in V}(w_V^p\boldsymbol{f}^{pq} + w_V^q\boldsymbol{f}^{qp})\otimes\boldsymbol{x}^c \\ &= \frac{1}{V}\sum_{c\in\partial V}(w_V^p - w_V^q)\,\boldsymbol{f}^c\otimes\boldsymbol{x}^c \;,\end{aligned} \tag{30}$$

since $w_V^p - w_V^q = 0$ when both particles are completely inside V. Note that every contact is visited once in Eq. (30) but twice in Eqs. (28) and (29). The expression $c \in \partial V$ means for the particle-center averaging method that contacts contribute only if one particle is inside V while the other is outside. In the framework of the slicing method, contacts contribute if at least one particle is cut by ∂V so that $w_V^p - w_V^q \neq 0$.

Given an arbitrary averaging volume V, and all the information about the forces at all contacts from the discrete element simulations, it is obvious that – from the technical point of view – the sum in Eq. (28) can be done relatively easily, whereas the sum in Eq. (30) requires the identification of the contacts at the "surface" of V, before the possibly shorter summation can be performed. Note that both expressions Eq. (28) and Eq. (30) have been used by different authors, see e.g. [6, 9, 31].

The values of the volumetric stress $\sigma_V = \mathrm{tr}(\boldsymbol{\sigma})$, the deviatoric fraction $\sigma_D/\sigma_V = \mathrm{dev}(\boldsymbol{\sigma})/\mathrm{tr}(\boldsymbol{\sigma})$, as obtained from our simulations, are plotted in Figs. 8(a-b). The volumetric stress is constant, besides fluctuations, whereas the deviatoric fraction is rather large in the shear-zone and decays with increasing distance from the inner ring, like the fabric. Also, the deviatoric fraction of the stress appears slightly reduced in magnitude for increasing global density. Note that the stress varies over almost two orders of magnitude, while the mean density is changed only weakly from $\bar{\nu} = 0.8084$ to 0.8194, see table 2. In Fig. 8c ϕ_σ describes the angle which the principal axis of the stress tensor is tilted from the outward direction. The stress tensor is, on average, rotated counter clockwise by somewhat less than $\pi/4$ from the outward direction. It is only in the outermost part that strong fluctuations exist around the mean. We now provide evidence that the fabric and stress are *not* co-linear.

4.3 Mean strain tensor

To achieve the material properties of a granular ensemble one is interested in the stress-strain relationship of the material. One of the simplest techniques used, is the application of "Voigt's hypothesis" which assumes that the strain is uniform and that every particle displacement conforms to the mean displacement field [32]. Thus, the expected displacement at contact c of particle p, relative to the force free situation, and due to the mean displacement gradient $\boldsymbol{\epsilon}$, is $\boldsymbol{\epsilon} \cdot \boldsymbol{l}^{pc}$, with $\boldsymbol{l}^{pc} = a_p \boldsymbol{n}^c$, and the mean contact deformation δ. Note that the linear, symmetric strain $\boldsymbol{\varepsilon} = \frac{1}{2}(\boldsymbol{\epsilon} + \boldsymbol{\epsilon}^{\mathrm{T}})$ is not identical to the displacement gradient, in general. In our study, we follow the approach of Liao et al. [10], who used $\boldsymbol{l}^{pq}$ instead of $\boldsymbol{l}^{pc}$, and assume that the actual displacement field does not coincide with, but fluctuates about the mean displacement field. The difference between the actual displacement $\boldsymbol{\Delta}^{pc}$ and the expected displacement is

$$\boldsymbol{\chi}^{pc} = \boldsymbol{\epsilon} \cdot \boldsymbol{l}^{pc} - \boldsymbol{\Delta}^{pc} \ . \tag{31}$$

The actual displacement is directly related to the simulations via $\boldsymbol{\Delta}^{pc} = \delta^c \boldsymbol{n}^c$.

If one assumes that the mean displacement field best approximates the actual displacement, one can apply a "least square fit" to the total fluctuations

$$S = \frac{1}{V} \sum_{p \in V} w_V^p \sum_{c=1}^{\mathcal{C}^p} (\boldsymbol{\chi}^{pc})^2 \ , \tag{32}$$

by minimizing S with respect to the mean displacement gradient so that

$$\frac{\partial S}{\partial \boldsymbol{\epsilon}} \stackrel{!}{=} \mathbf{0} \tag{33}$$
$$= \frac{2}{V} \sum_{p \in V} w_V^p \sum_{c=1}^{\mathcal{C}^p} (\boldsymbol{\epsilon} \cdot \boldsymbol{l}^{pc} - \boldsymbol{\Delta}^{pc}) \cdot \frac{\partial}{\partial \boldsymbol{\epsilon}} (\boldsymbol{\epsilon} \cdot \boldsymbol{l}^{pc} - \boldsymbol{\Delta}^{pc}) \ .$$

These four equations for the four components of $\boldsymbol{\epsilon}$ in 2D can be transformed into a relation for the mean displacement tensor as a function of the contact displacements and the branch vectors. By assuming that $\partial \boldsymbol{\Delta}^{pc}/\partial \boldsymbol{\epsilon} = \mathbf{0}$, the expression "$\cdot \frac{\partial}{\partial \boldsymbol{\epsilon}} (\boldsymbol{\epsilon} \cdot \boldsymbol{l}^{pc})$" becomes a dyadic product "$\otimes \boldsymbol{l}^{pc}$", as can be seen by writing down the equation in index notation. Extracting $\boldsymbol{\epsilon}$ from the sum (what leaves $\boldsymbol{l}^{pc} \otimes \boldsymbol{l}^{pc}$, the core of the fabric, in the first term) and multiplying the equation with $\mathbf{A} = \mathbf{F}^{-1}$, the inverse of the fabric, see Eq. (15), we find that

$$\boldsymbol{\epsilon} = \frac{\pi h}{V} \left(\sum_{p \in V} w_V^p \sum_{c=1}^{\mathcal{C}^p} \boldsymbol{\Delta}^{pc} \otimes \boldsymbol{l}^{pc} \right) \cdot \mathbf{A} \ . \tag{34}$$

The values of ϵ_V, ϵ_D/ϵ_V, and ϕ_ϵ, as obtained from our simulations, are plotted in Figs. 9(a-c). The elastic, volumetric deformation gradient of the granulate is localized in the shear zone and the effect is stronger in the less dense systems. Due to dilation it is easier to compress the dilute material closer to the inner ring compared to the outer part. Like the fabric and stress, the strain also becomes more isotropic with increasing mean density.

5 Results

At first, we compute the mean-field expectation values for $\boldsymbol{\sigma}$ and $\boldsymbol{\epsilon}$, in order to get a rough estimate for the orders of magnitude of the following results. Replacing, in Eq. (28), f^c by its mean $\bar{f} = k_n \bar{\delta}$, a_p by $a = \bar{a}$, and $\boldsymbol{l}^{pc}$ by $a\boldsymbol{n}^c$, one gets

$$\bar{\boldsymbol{\sigma}} = (k_n \bar{\delta}/\pi a)\, \mathbf{F} \ . \tag{35}$$

Performing some similar replacements in Eq. (34), leads to

$$\bar{\boldsymbol{\epsilon}} = (\bar{\delta}/a)\, \mathbf{I} \ , \tag{36}$$

or

$$\bar{\boldsymbol{\epsilon}} = (\pi/k_n)\, \boldsymbol{\sigma} \cdot \mathbf{A} \ . \tag{37}$$

The material stiffness, $\bar{E}$, can be defined as the ratio of the volumetric parts of stress and strain, so that one obtains from Eq. (35) and (36)

$$\bar{E} = (k_n/2\pi)\, \mathrm{tr}(\mathbf{F}) \ . \tag{38}$$

In Fig. 10 the rescaled stiffness of the granulate is plotted against the trace of the fabric for all simulations. Note

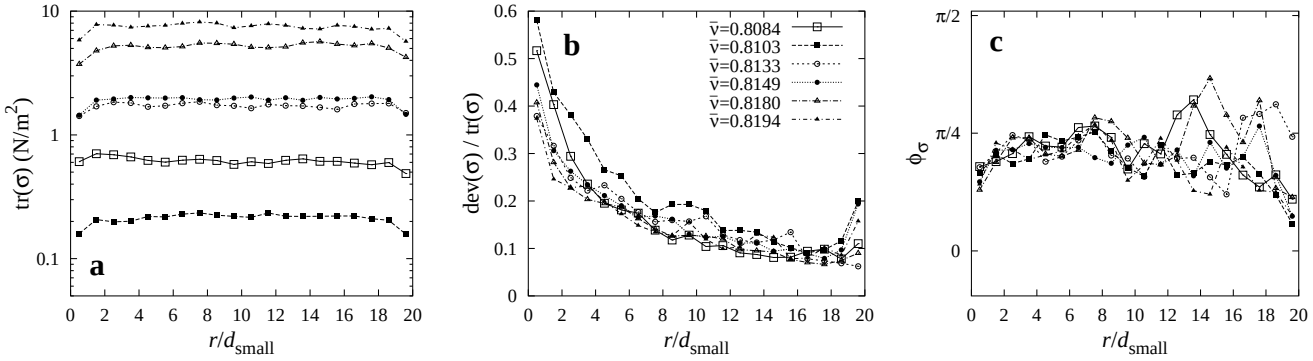

Fig. 8. a-c Plot of (**a**) $\sigma_V = \mathrm{tr}(\boldsymbol{\sigma})$, (**b**) $\sigma_D/\sigma_V = \mathrm{dev}(\boldsymbol{\sigma})/\mathrm{tr}(\boldsymbol{\sigma})$, and (**c**) ϕ_σ against the dimensionless distance r/d_{small} from the inner ring, as obtained with the slicing method. The global volume fraction is given in (**b**) and valid also for (**a**) and (**c**).

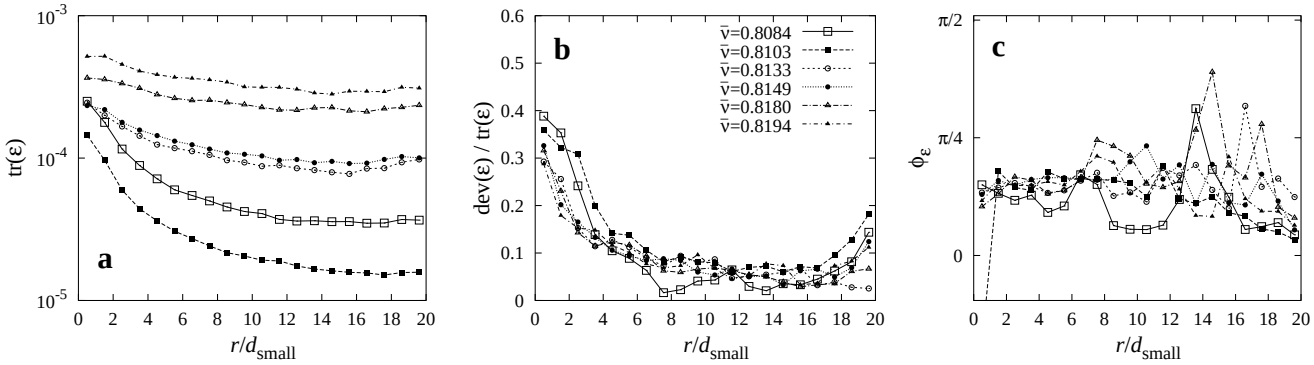

Fig. 9. a-c Plot of (**a**) $\epsilon_V = \mathrm{tr}(\boldsymbol{\epsilon})$, (**b**) $\epsilon_D/\epsilon_V = \mathrm{dev}(\boldsymbol{\epsilon})/\mathrm{tr}(\boldsymbol{\epsilon})$, and (**c**) ϕ_ϵ against the dimensionless distance r/d_{small} from the inner ring. The global volume fraction is given in (**b**) and valid also for (**a**) and (**c**).

that all data collapse almost on a line, but the mean-field value underestimates the simulation data by a few percent. Simulation data for different k_n and even data from simulations with neither bottom- nor tangential friction collapse with the data for fixed k_n and different volume fractions, shown here. The deviatoric fraction of $\boldsymbol{\sigma}$ is plotted in Fig. 11 against the deviatoric fraction of $\mathbf{F}$. Here, the data are strongly underestimated by the mean-field result in Eq. (35). A similar plot for the deviatoric fraction of the deformation gradient against F_D/F_V shows a gathering of the data close to the identity curve, in disagreement with Eq. (36). Thus, we conclude that the deviatoric parts of stress, deformation gradient and fabric are interconnected in a more complicated way than suggested by the simple mean field estimates [9, 32, 34, 35].

In Fig. 12 the ratio of the deviatoric parts of stress and strain is plotted against the trace of the fabric. Like the material stiffness, both quantities are proportional, only G shows much stronger fluctuations and has a proportionality factor of about 1/3. We did not use the traditional

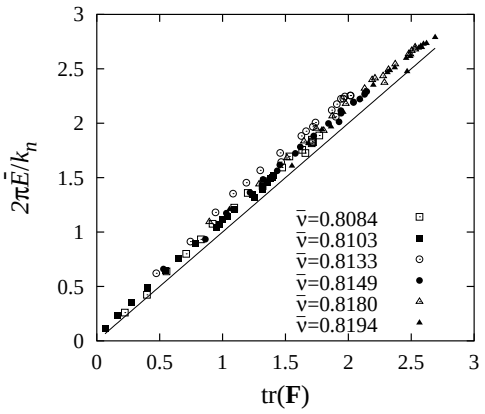

Fig. 10. Granulate stiffness $2\pi\bar{E}/k_n = \mathrm{tr}(\boldsymbol{\sigma})/\mathrm{tr}(\boldsymbol{\epsilon})$, plotted against $\mathrm{tr}(\mathbf{F})$ from all simulations.

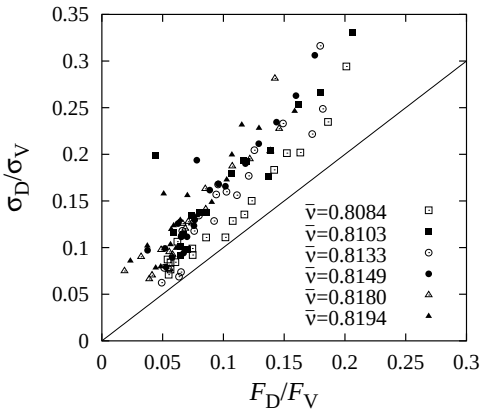

Fig. 11. Deviatoric fraction $\mathrm{dev}(\boldsymbol{\sigma})/\mathrm{tr}(\boldsymbol{\sigma})$ plotted against $\mathrm{dev}(\mathbf{F})/\mathrm{tr}(\mathbf{F})$ from all simulations.

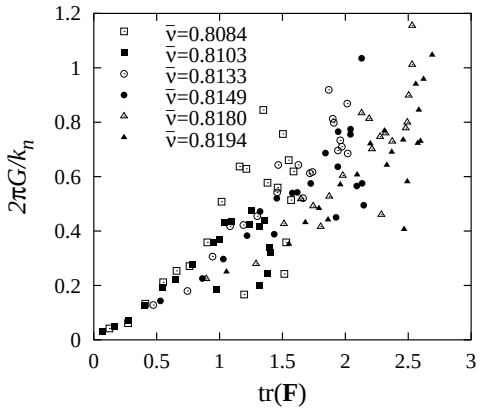

Fig. 12. Scaled granulate shear resistance $G = \mathrm{dev}(\boldsymbol{\sigma})/\mathrm{dev}(\boldsymbol{\epsilon})$ plotted against $\mathrm{tr}(\mathbf{F})$ from all simulations.

definition of the shear modulus [9], since our tensors are not co-linear as shown below.

In Fig. 13 the orientations of the tensors are plotted for some simulations and in the inner part of the shear cell. In the outer part, the deviatoric fraction is usually around 10 per-cent, i.e. so small that the orientations become noisier. Simulations A and B are skipped here, because the data of the orientations are rather noisy due to the low density which leads to intermittent behavior with strong fluctuations. We observe that all orientation angles ϕ show the same qualitative behavior, however, the fabric is tilted more than the stress which in turn is tilted more than the deformation gradient, where the orientations are measured in counter clockwise direction from the radial outward direction.

As a final cross-check, inserting the measured values for $\boldsymbol{\sigma}$ and $\mathbf{A}$ into Eq. (37) leads to the measured values of $\boldsymbol{\epsilon}$ within a few percent deviation. However, the orientation of the deformation gradient is not well reproduced – it seems very sensitive to small fluctuations.

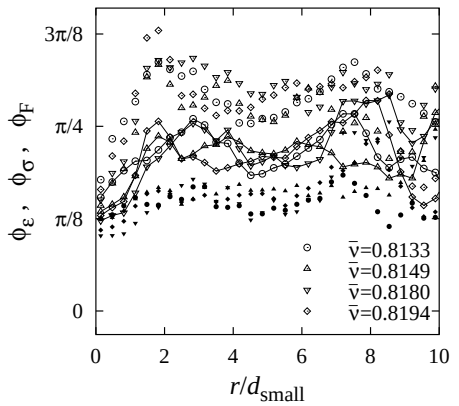

Fig. 13. Orientation of the tensors $\mathbf{F}$, $\boldsymbol{\sigma}$, and $\boldsymbol{\epsilon}$ plotted against r/d_{small} from simulations C, D, E, and F with $B_s = 60$. The data are shown in the range $0 \leq r/d_{\mathrm{small}} \leq 10$ only. Open symbols are fabric, open symbols connected by lines are stress, and solid symbols are strain, the mean densities corresponding to the symbols is given in the plot.

6
Summary and Conclusion

Discrete element simulations of a 2D Couette shear cell were presented and used as the basis for a micro-macro averaging procedure. In the shear cell a shear band is localized close to the inner, rotating cylindrical wall. The boundary conditions were chosen to allow for averaging over large volumes (rings with width Δr) and over a steady state and thus over long times. The configurations changed rather rapidly in the shear band, whereas the system is frozen in the outer part, a fact which requires either extremely long simulations or a sampling over different initial conditions in order to allow an ensemble averaging in the outer part.

The simplest averaging strategy involves only the particle-centers as carriers of the quantities to be averaged over, whereas a more advanced method assumes the quantities to be homogeneously smeared out over the whole particle which is cut in slices by the averaging volumes. Both methods agree if the averaging volumes are of the particle size (or multiples), but for other sizes differing results are obtained. The slicing method shows discretization effects in the range of averaging volume widths from one to one fifth of a particle diameter, while the particle-center method shows fluctuations due to the choice of the averaging volume in a much wider range.

The material density, i.e. the volume fraction, the coordination number, the fabric tensor, the stress tensor and the elastic, reversible deformation gradient were obtained by the averaging procedures. The fabric is linearly proportional to the product of volume fraction and coordination number. In the shear band, dilation together with a reduction of the number of contacts is observed. The mean stress is constant in radial direction while the deformation gradient decays with the distance from the inner wall. The ratio of the volumetric parts of stress and strain gives the effective stiffness of the granulate, which is small in the shear band and larger outside, due to dilation.

In the shear band, large deviatoric components of all tensorial quantities are found, however, decreasing with increasing distance from the inner wall. The isotropy of the tensors grows only slightly with increasing density and all tensors are tilted counterclockwise from the radial direction by an angle of the order of $\pi/4$. The system organizes itself such that more contacts are created to act against the shear. An essential observation is that the macroscopic tensors are *not* co-linear, i.e. their orientations are different. The orientation of the fabric is tilted most, that of the deformation gradient is tilted least and thus, the material cannot be described by a simple elastic model involving only two Lamé constants (or bulk modulus and Poisson's ratio) as the only parameters. Alternatives are to cut the system into pieces with different material properties and thus introducing discontinuities [1] or to use the rank four stiffness tensor for anisotropic materials [35]. The deviatoric parts of stress and deformation gradient are seemingly interconnected via the fabric tensor.

To conclude, we proposed a consistent averaging formalism to obtain a mean quantity Q in average over arbitrary volumes V. Within this framework, we used for Q^c the fabric $\mathbf{F}^c = \boldsymbol{n}^c \otimes \boldsymbol{n}^c$, the stress $\boldsymbol{\sigma}^c = (1/V^p)\boldsymbol{f}^c \otimes \boldsymbol{l}^{pc}$,

and the deformation gradient $\boldsymbol{\epsilon}^c = (\delta^c/a_p)\boldsymbol{n}^c \otimes \boldsymbol{n}^c \cdot \mathbf{A}$. Future work will involve the extension of the present analysis to measure also the fluctuations of the above quantities and, in addition, other interesting quantities like, e.g. , the plastic strain and non-symmetric parts of the stress tensor due to the effective moments acting on single particles. More systematic parameter studies are currently in progress.

References

1. H. J. Herrmann, J.-P. Hovi, and S. Luding, editors. *Physics of dry granular media - NATO ASI Series E 350*. Kluwer Academic Publishers, Dordrecht, 1998.
2. P. A. Cundall and O. D. L. Strack. A discrete numerical model for granular assemblies. *Géotechnique*, 29(1):47–65, 1979.
3. A. Drescher and G. de Josselin de Jong. Photoelastic verification of a mechanical model for the flow of a granular material. *J. Mech. Phys. Solids*, 20:337–351, 1972.
4. L. Rothenburg and A. P. S. Selvadurai. A micromechanical definition of the cauchy stress tensor for particulate media. In A. P. S. Selvadurai, editor, *Mechanics of Structured Media*, pages 469–486. Elsevier, 1981.
5. S. B. Savage and D. J. Jeffrey. The stress tensor in a granular flow at high shear rates. *J. Fluid. Mech.*, 110:255, 1981.
6. P. A. Cundall, A. Drescher, and O. D. L. Strack. Numerical experiments on granular assemblies; measurements and observations. In *IUTAM Conference on Deformation and Failure of Granular Materials*, pages 355–370, Delft, 1982.
7. J. D. Goddard. Microstructural origins of continuum stress fields - a brief history and some unresolved issues. In D. DeKee and P. N. Kaloni, editors, *Recent Developments in Structered Continua. Pitman Research Notes in Mathematics No. 143*, page 179, New York, 1986. Longman, J. Wiley.
8. R. J. Bathurst and L. Rothenburg. Micromechanical aspects of isotropic granular assemblies with linear contact interactions. *J. Appl. Mech.*, 55:17, 1988.
9. N. P. Kruyt and L. Rothenburg. Micromechanical definition of strain tensor for granular materials. *ASME Journal of Applied Mechanics*, 118:706–711, 1996.
10. C.-L. Liao, T.-P. Chang, D.-H. Young, and C. S. Chang. Stress-strain relationship for granular materials based on the hypothesis of best fit. *Int. J. Solids Structures*, 34:4087–4100, 1997.
11. I. Goldhirsch. Note on the definition of stress for discrete systems. preprint, 1999.
12. E. Kuhl, G. A. DÁddetta, H. J. Herrmann, and E. Ramm. A comparison of discrete granular material models with continuous microplane formulations. *Granular Matter*, 2/3, 2000. in press.
13. O. R. Walton. Numerical simulation of inelastic, frictional particle-particle interactions. In M. C. Roco, editor, *Particulate two-phase flow*, page 884, Boston, 1993. Butterworth-Heinemann.
14. G. Lian, M. J. Adams, and C. Thornton. Elastohydrodynamic collisions of solid spheres. *J. Fluid Mech.*, 311:141, 1996.
15. S. F. Foerster, M. Y. Louge, H. Chang, and K. Allia. Measurements of the collision properties of small spheres. *Phys. Fluids*, 6(3):1108–1115, 1994.
16. L. Labous, A. D. Rosato, and R. Dave. Measurements of collision properties of spheres using high-speed video analysis. *Phys. Rev. E*, 56:5715, 1997.
17. E. Falcon, C. Laroche, S. Fauve, and C. Coste. Behavior of one inelastic ball bouncing repeatedly off the ground. *Eur. Phys. J. B*, 3:45–57, 1998.
18. H. Hertz. Über die Berührung fester elastischer Körper. *J. für die reine u. angew. Math.*, 92:136, 1882.
19. L. D. Landau and E. M. Lifshitz. *Elasticity Theory*. Pergamon Press, Oxford, 1975.
20. P. A. Cundall and O. D. L. Strack. Modeling of microscopic mechanisms in granular materials. In J. T. Jenkins and M. Satake, editors, *Mechanics of Granular Materials: New Models and Constitutive Relations*, pages 137–149, Amsterdam, 1983. Elsevier.
21. M. Lätzel, S. Luding, and H. J. Herrmann. Dependence of macroscopic material properties on microscopic model parameters. in preparation, 2000.
22. S. Schöllmann. Simulation of a two-dimensional shear cell. *Phys. Rev. E*, 59(1):889–899, 1999.
23. D. Howell and R. P. Behringer. Fluctuations in a 2d granular Couette experiment: A critical transition. *Phys. Rev. Lett.*, 82:5241, 1999.
24. C. T. Veje, D. W. Howell, R. P. Behringer, S. Schöllmann, S. Luding, and H. J. Herrmann. Fluctuations and flow for granular shearing. In H. J. Herrmann, J.-P. Hovi, and S. Luding, editors, *Physics of Dry Granular Media*, page 237, Dordrecht, 1998. Kluwer Academic Publishers.
25. C. T. Veje, D. W. Howell, and R. P. Behringer. Kinematics of a 2D granular Couette experiment. *Phys. Rev. E*, 59:739, 1999.
26. J. D. Goddard. Continuum modeling of granular assemblies. In H. J. Herrmann, J.-P. Hovi, and S. Luding, editors, *Physics of Dry Granular Media*, pages 1–24, Dordrecht, 1998. Kluwer Academic Publishers.
27. S. C. Cowin. A simple thoery of instantaneously induced anisotropy. In J. T. Jenkins and M. Satake, editors, *Micromechanics of Granular Materials*, pages 71–80, Amsterdam, 1988. Elsevier.
28. O. Tsoungui, D. Vallet, and J.-C. Charmet. Use of contact area trace to study the force distributions inside 2d granular systems. *Granular Matter*, 1(2):65–69, 1998.
29. P. Dubujet and F. Dedecker. Micro-mechanical analysis and modelling of granular materials loaded at constant volume. *Granular Matter*, 1(3):129–136, 1998.
30. M. M. Mehrabadi, S. Nemat-Nasser, H. M. Shodja, and G. Subhash. Some basic theoretical and experimental results on micromechanics of granular flow. In *Micromechanics of granular media*, Amsterdam, 1988. Elsevier.
31. C. S. Chang. Micromechanical modelling of constitutive relations for granular media. In *Micromechanics of granular media*, Amsterdam, 1988. Elsevier.
32. C.-L. Liao and T.-C. Chang. A generalized constitutive relation for a randomly packed particle assembly. *Computers and Geotechnics*, 20(3/4):345–363, 1997.
33. O. Tsoungui, M. Lätzel, S. Luding, and H. J. Herrmann. Influence of the particle size distribution function on the material properties of granular media. in preparation, 2000.
34. S. Luding, M. Lätzel, W. Volk, S. Diebels, and H. J. Herrmann. From discrete element simulations to a continuum model. European Congress on Computational Methods in Applied Sciences and Engineering, ECCOMAS, Barcelona 2000.

35. S. Luding and M. Lätzel. Non-colinearity of stress and strain in the presence of anisotropic contact networks. in preparation, 2000.